Comparative Study for Corrosion Resistance of Ferrous and Non-ferrous Pipes Immersed in Magnetized Water

Bilal Ali Abbas AL-HALBOOSI, İsmail Hakkı KARA *

Metallurgy and Materials Engineering Department of Engineering Faculty, Karabük University, Karabük,78050, Turkey

http://doi.org/10.5755/j02.ms.36247

Received 2 February 2024; accepted 2 September 2024

This study aims to investigate the corrosion resistance of galvanized steel (GS) and AZ31 pipe materials immersed in a magnetized water treatment (MWT) applied river water source. The potentiodynamic corrosion test results showed that a better corrosion rate is obtained by the AZ31(corr.rate: 0.0442 mm/y) specimen than GS (corr.rate: 0.0764 mm/y) due to the passivation efficiency resulting from the calcite and MgO particles on the surface.
Keywords: AZ31, galvanized steel, magnetized water treatment, corrosion.

1. INTRODUCTION

In recent years, studies aimed at reducing the hardness of water with the magnetized water method have attracted attention [1]. In addition, studies on the effects of magnetized water with changed properties in different areas are increasing [2]. The magnetic water method is preferred because it is cheap and chemical-free [3]. Many studies have used and examined the magnetic water method to reduce the tendency of water to form calcite or to develop more efficient products [4]. However, there are very few studies on the effects or damage of magnetized water on carrier systems. Wenlu Yang et al. investigated the galvanic corrosion behavior of AZ91D in distilled water and they stated that the galvanic current density increases with increasing temperature and soaking time, which can be attributed to the damage of the corrosion product film due to hydrogen release [5]. Zhen Xu et.al. tested magnesium alloy in different media to test the corrosion behavior after solution treatment, where they found that Mg corrosion in solvents increased in the order: low pH > saline pH > high pH and Mg corrosion products are mainly $Mg(OH)_2$ and MgO [6].

The costs incurred due to corrosion in agricultural structures in the USA and China have been reported to be around 1.1 billion and 9.89 billion dollars [7, 8]. $CaCO_3$ in aragonite formation is stored in micro cathodic regions and provides the formation of fewer cathodic regions where iron ions cannot reach. $CaCO_3$/interlayer composite coating formed in Mg alloy may be suitable to reduce corrosion losses in agricultural applications [9].

This study tested galvanized steel pipe and AZ31 Mg pipe samples for corrosion in magnetized river water. Potentiodynamic corrosion test results were compared, and corrosion products were examined.

2. EXPERIMENTAL DETAILS

Water types and their chemical contents are given in Table 1. Inductively coupled plasma-optical emission spectrometry (ICP-OES) determined the chemical composition of the water. As to Magnetization Treatment, a 2 T magnetic field with a magnet speed of 0.45 m/s was utilized. The surface morphology of specimens after SEM obtained corrosion equipped with EDX analysis.

Table 1. Chemical analysis of waters.

Normal river water		Magnetized river water	
Element	mg/l	Element	mg/l
Mg	20	Mg	4.5
Ca	15	Ca	10
Na	4.7	Na	4.6
K	0.13	K	0.08
Cl	10	Cl	4.5
HCO_3	6.5	HCO_3	10
SO_4	4.9	SO_4	5.7
pH	7.43	pH	7.52

The specimens were placed in normal water and magnetized water for 192 hours. Replacement of magnetized water with new magnetized water was made every 24 hours. The potentiostat setup includes a Host computer, thermostat, magnetic stirrer, (EmStat 4s, Palm Sens, Holland) potentiostat, and galvanostat. The cell is (250 ml) capacity made of Pyrex and consists of internal and external bowls. The electrochemical corrosion cell has three electrodes. Carbon steel as a working electrode is used to determine the potential according to the reference electrode, an auxiliary electrode is platinum with length (10 cm), and the reference electrode is a saturated calomel (Hg/Hg_2Cl_2 sat. KCl). The working electrode was immersed in the test solution for 15 min to establish steady-state open circuit potential, then electrochemical measurements were performed in a potential range of ± 200 mV. All tests were carried out at 298 K by using a cooling-heating circulating water bath.

* Corresponding author. Tel.: +90-(370)418-7050; fax: +90 (370)418-7051. E-mail: *ihakkikara@karabuk.edu.tr* (I.H. Kara)

3. RESULTS AND DISCUSSION

Table 1 shows a chemical analysis result of MWT-applied waters. In Fig. 1, the SEM images show the surface of corroded steel pipe and AZ31 specimens in normal river water and MWT one. As a morphological, the SEM images show block-like particles agglomerated on the surface of both the steel pipe and AZ31 specimen which was obtained after corrosion in MWT water. However, the specimens that were exposed to corrosion in non-MWT water had smoother surfaces. These equiaxed particles are calcite formed as Ca $(CO)_3$ [10].

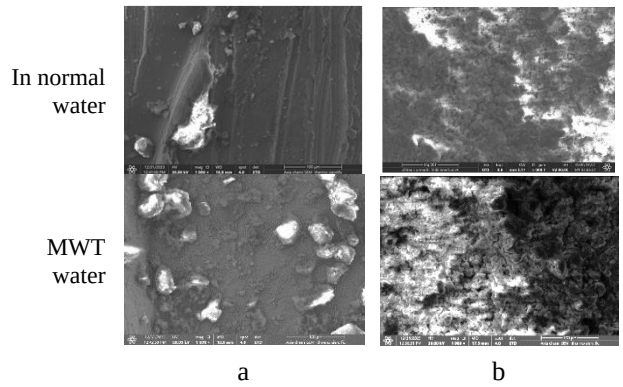

Fig. 1. SEM images of degradation on the surface of specimens: a – galvanized steel; b – AZ31

Table 2 and Table 3 illustrate the elements on the surface of specimens exposed to corrosion in river water and MWT-applied river water sources.

Table 2. Chemical analysis of corroded surfaces of specimens in normal river water

Element	Atomic mass, %	Element	Atomic mass, %
Galvanized steel		AZ31	
C	35.8 ± 0.3	C	16.8 ± 0.2
O	33.0 ± 0.3	O	63.9 ± 0.5
Mg	1.8 ± 0.1	Mg	1.5 ± 0.0
Al	–	Al	0.3 ± 0.0
Si	2.0 ± 0.0	Si	0.9 ± 0.0
Ca	3.4 ± 0.0	Ca	16.1 ± 0.1
Fe	–	Fe	0.2 ± 0.0
Zn	25.1 ± 0.1	Zn	0.3 ± 0.0

Table 3. Chemical analysis of corroded surfaces of specimens in MWT-applied river water

Element	Atomic mass, %	Element	Atomic mass, %
Galvanized steel		AZ31	
C	23.0±0.4	C	15.8±0.1
O	45.6±0.3	O	64.6±0.5
Mg	1.8±0.1	Na	0.8±0.0
Al	2.1±0.1	Mg	2.5±0.0
Si	7.9±0.1	Si	0.5±0.0
Cl	0.2±0.0	Ca	15.6±0.1
Ca	2.4±0.0	Fe	0.2±0.0
Fe	0.7±0.0		
Ni	0.1±0.0		
Zn	15.9±0.1		

Oxidation occurs on the galvanized steel surface containing Ca, C, and O elements forming as Ca $(CO)_3$ (ΔH = -1206.9 kJ mol^{-1}) [11]. In addition, Zn, Mg, and Al are detected, where ZnO (ΔH = -350.5 kJ mol^{-1}) formation is lower than MgO (ΔH = -532.61 kJ mol^{-1}) and Al_2O_3 (ΔH = -1620.6 kJ mol^{-1}) [11]. Similarly, the corroded surface of the AZ31 specimen is mainly occupied by Ca $(CO)_3$ and MgO particles. It is seen that the Ca and Mg contents of the corroded AZ31 surface as atomic mass % are higher than the corroded surface of galvanized steel.

Fig. 2 and Fig.3 show Tafel curves obtained from potentiodynamic corrosion test results in Normal water (NW) of galvanized steel and AZ31 Mg, respectively.

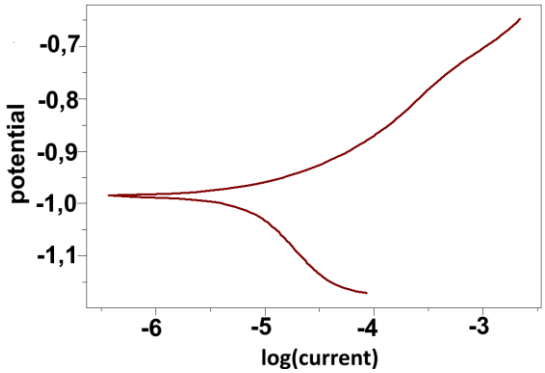

Fig. 2. Tafel curve of galvanized steel specimen in normal water

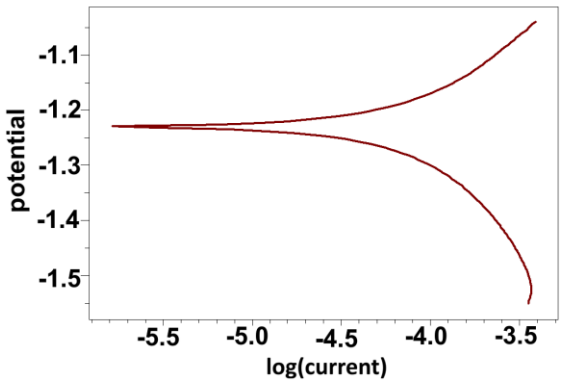

Fig. 3. Tafel curve of AZ31 specimen in normal water

It is measured that the corrosion rate of AZ31 is higher than galvanized steel. The corrosion rate was measured as 0.45260 mm/y and 0.07794 mm/y for AZ31 and GS, respectively. The higher Zn and Mg content of GS material enables the formation of calcite and ZnO and MgO particles on the surface, where the polarization resistance may be the reason for the better corrosion resistance for GS (see Table 3). It is said that the lesser Ecorr values indicate higher susceptibility. In comparison, higher Ecorr values (toward the positive side) indicate inertness toward the corrosive Cl^- ion medium for ZnO-Mg Coating on AISI 4140 Steel [12].

Fig.4 and Fig.5 show Tafel curves obtained from potentiodynamic corrosion test results of galvanized steel and AZ31 Mg, respectively. It is measured that the corrosion rate of AZ31 is lower than galvanized steel. The corrosion rate of AZ31 was lower than the galvanized steel at 0.04421 mm/y and 0.07642 mm/y, respectively.

The more Ca and Mg content of AZ31 material enables the formation of calcite and MgO particles on the surface, where the passivation mechanism could be the reason for the better corrosion resistance for AZ31. Moreover, it is seen that the PE% (inhibition efficiency %) value of AZ31

was obtained as 90.23 but the value of galvanized steel is 1.93 (see Table 4).

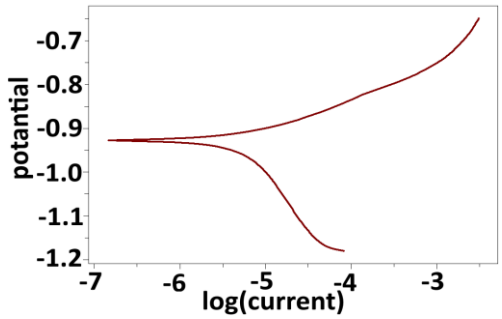

Fig. 4. Tafel curve of galvanized steel specimen in MWT applied water

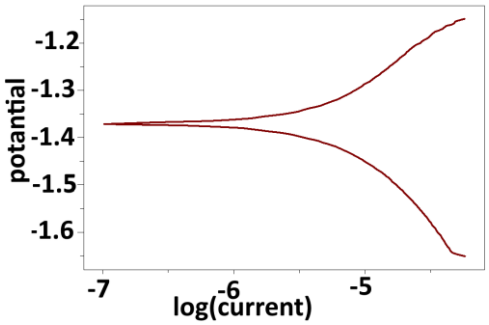

Fig. 5. Tafel curve of AZ31 specimen in MWT applied water

Table 4. Corrosion test results of samples

	Ecorr, mV	Icorr, mA/cm^2	CR, mm/y	Rp, Ω/cm^2	*PE*%
GS in NW	986.60	0.006710	0.07794	4197	-
AZ31 in NW	1220.9	0.038970	0.45260	866.3	-
GS in MWT	961	0.00658	0.07640	4483	1.93
AZ31 in MWT	1364	0.00380	0.04420	11080	90.23

Moreover, it is stated that the low solubility of $CaCO_3$ promotes the continuous progress of the reaction of $Ca^{2+} + CO_2^{-3} \rightarrow CaCO_3$, thus leaving increased H+ in the solution and a decreased solution pH which was seen in the un-MWT solution, where it is observed that the presence of Ca^{2+} promotes the acidification of the solution and accelerates the dissolution of the P110 steel [13]. The GS corrosion rate in the solution of normal river water was obtained lower than in the solution of MWT applied one.

Fig. 6 presents EDX results obtained from the corroded surface of GS and AZ31 in normal water. As seen in Fig. 6, the main difference is the Zn particle distribution on the surfaces of GS and AZ31 specimens. Almost Zn occupied all sections of the surface on GS. Also, the dark region that was not occupied by Zn was dominated by Ca. Thus, we can say that the mutual effects of Zn and Ca distribution could be the reason for the better corrosion rate of galvanized steel.

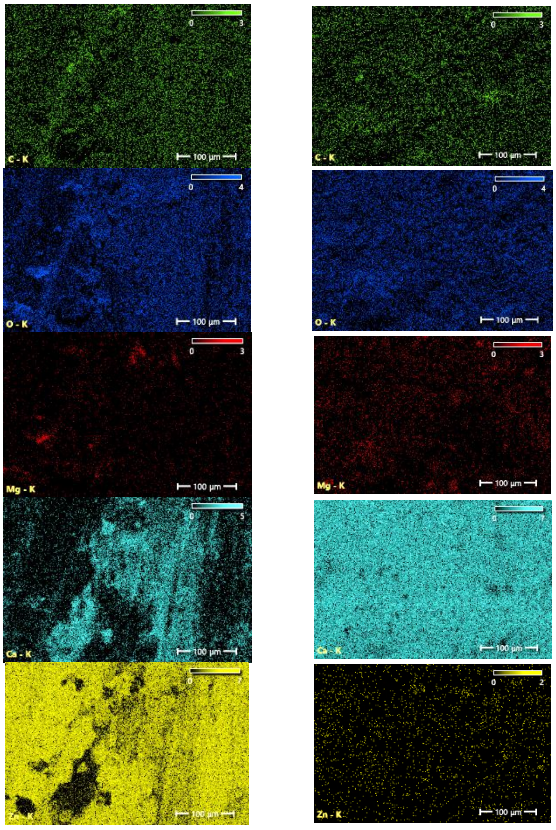

a b

Fig. 6. EDX analysis obtained from corroded surfaces of specimens immersed in normal water: a – galvanized steel; b – AZ31

Fig. 7 shows EDX results obtained from the corroded surface of GS and AZ31. As seen in Fig. 7, The oxidation on the surface of AZ31 distributed almost all sections of the area, but the GS specimen contains more non-oxidized sections as dark islands. Similarly, the spreading of Mg particles on the AZ31 surface is homogeneous and consists of fewer dark regions than GS. As to, the Ca particles that spread over the whole of that region of AZ31, where there is a bigger difference when we compare it with GS which contains blacker sections. The difference in Zn particle distribution is mainly the separately homogeneous spreading on AZ31. However, closer Zn particles with each other dominate in some sections of GS. The pitting corrosion formation that is reported as rare in pH 7.4 environments due to the MgO-$Mg(OH)_2$ passivation layer has better stability, which results in the formation of a thicker $Mg(OH)_2$ layer on the surface of the magnesium alloy, thus improving the passivation effect of the layer[14]. It is seen from Fig.8, that the image of Ca deposited surface of AZ31 includes very little pitting corrosion. The Ca $(CO)_3$ and MgO Pourbaix diagrams were produced based on the ion concentrations taken from Table 2 [15] and [16] Fig. 8 shows $Ca(CO)_3$ Pourbaix diagram where ion concentrations of Ca and C are 0.156 and 0.158, respectively. In Fig. 9, the Mg ion concentration is 0.025, we can see MgO stability after pH 11.70. However, $Ca(CO)_3$ stability is observed after pH 4. AZ31 specimen immersed in the river water, measured pH value of river water is pH 7.4, has more effective passivity of $Ca(CO)_3$ than MgO.

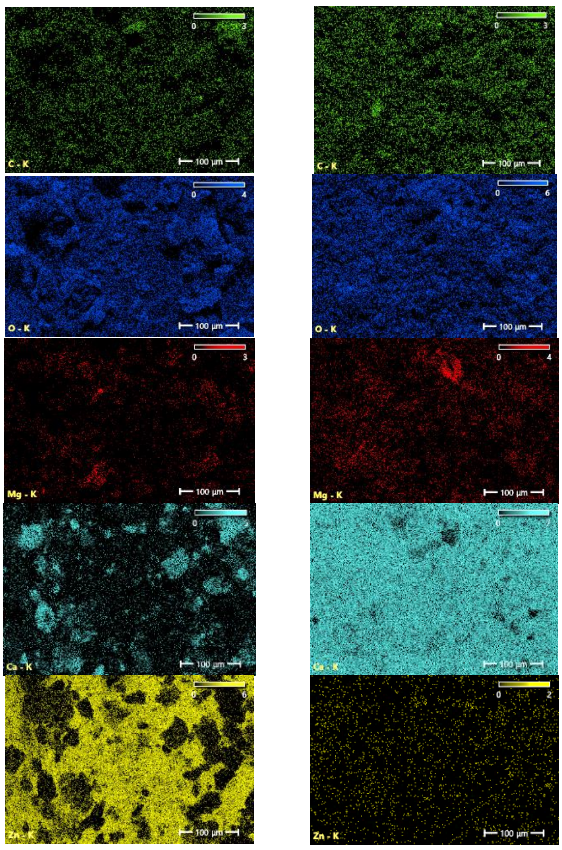

a b

Fig. 8. EDX analysis obtained from corroded surfaces of specimens immersed in MWT water: a – galvanized steel; b – AZ31

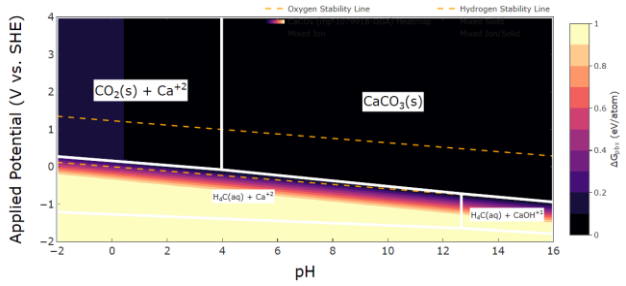

Fig. 9. Pourbaix Diagram of $Ca(CO)_3$ drawing for chemical analysis of corroded surfaces of AZ31 [15] and [16]

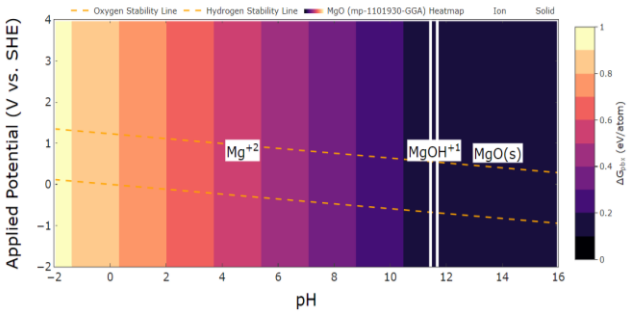

Fig. 10. Pourbaix Diagram of MgO drawing for chemical analysis of corroded surfaces of AZ31 [15] and [16]

Zhen Xu and et.al. tested magnesium alloy in different media to test the corrosion behavior after solution treatment, where they found that Mg corrosion in solvents increased in the order: low pH > saline pH > high pH and Mg corrosion products are mainly $Mg(OH)_2$ and MgO [6]. It is known that increasing mg ions in carbonate solution transforms the single-crystal calcite structure into an aggregate crystal structure. It has been said that increasing pH and mg ions cause faster nucleation and accumulation of $CaCO_3$. Due to increasing immersion time, the $CaCO_3$-covered area on the magnesium alloy increased. Finally, a continuous calcite $CaCO_3$/interlayer composite coating was formed on the surface of the Mg alloy [17].

In addition, the outer part of this composite coating consists of $CaCO_3$ and the inner part consists of Mg(Al)O layer. The coating system has a dense outer $CaCO_3$ layer and the inner Mg(Al)O layer shows the best corrosion resistance. The outer $CaCO_3$ layer can protect for the inner passivation film when embedded in Cl-containing content. AZ31 Mg alloy contributes to the corrosion resistance of the composite layer due to the Al element it contains. Wang Ye et al. An anticorrosive double-layer $CaCO_3$/Mg(Al)O coating system was prepared on AZ41 Mg alloy. The outer $CaCO_3$ has been shown to play a dual role in anti-corrosion and protection of the inner layer. In addition, it has been reported that the first layer of Mg(Al)O passivation film can survive and regenerate in corrosive environments. A "dissolution – repassivation" cycle behavior has been described here and has been reported to have an inhibitory or reducing effect on corrosion. [18].

4. CONCLUSIONS

The formation of particles such as calcite and oxides of Zn, Al, and Mg make an important contribution to the corrosion resistance of materials used in agricultural systems. AZ31 Mg pipe showed better corrosion resistance than galvanized steel pipe due to the passivation behavior of Mg and Calcite oxide particles in MWT-applied water.

REFERENCES

1. **Mahasti, N.N.N., Shih, Y.J., Vu, X.T., Huang, Y.H.** Removal of Calcium Hardness from Solution by Fluidized-bed Homogeneous Crystallization (FBHC) Process *Journal of the Taiwan Institute of Chemical Engineers* 78 2017: pp. 378 – 385. https://doi.org/10.1016/j.jtice.2017.06.040
2. **Hozayn, M., Abdallha, M.M., Abd, E.M.A., El-Saady, A.A., Darwish, M.A., Hozayn, M., Darwish, M.A.** Applications of Magnetic Technology in Agriculture: A Novel Tool for Improving Crop Productivity (1): Canola *African Journal of Agricultural Research* 11 (5) 2016: pp. 441 – 449. https://doi.org/10.5897/AJAR2015.9382
3. **Dobersek, D., Goricanec, D.** An Experimentally Evaluated Magnetic Device's Efficiency for Water-Scale Reduction on Electric Heaters *Energy* 77 2014: pp. 271 – 278. https://doi.org/10.1016/j.energy.2014.09.024
4. **Yunhan, W., Shengxian, C., Ye, Z., Yong, L., Huichao, Z.** Design of A Real-Time Monitoring System and Frequency Agility Electric Field Device to Prevent $CaCO_3$ Scaling on Heat Exchange Surfaces *Desalination* 565 2023: pp. 116850. https://doi.org/10.1016/j.desal.2023.116850

5. **Yang, W., Liu, Z., Huang, H.** Galvanic Corrosion Behavior Between AZ91D Magnesium Alloy and Copper in Distilled Water *Corrosion Science* 188 2021: pp. 109562. https://doi.org/10.1016/j.corsci.2021.109562

6. **Xu, Z., Eduok, U., Tiamiyu, A.A., Szpunar, J.** Anodic Dissolution Pattern of Magnesium Alloy in Different Media: Effects of Solution Treatment on Its Microstructure and Corrosion Behavior *Engineering Failure Analysis* 107 2020: pp. 104234. https://doi.org/10.1016/j.engfailanal.2019.104234

7. **Koch, G.H., Brongers, M.P., Thompson, N.G., Virmani, Y.P., Payer, J.H.** Cost of Corrosion in The United States *In Handbook Of Environmental Degradation Of Materials William Andrew Publishing* 2005: pp. 3 – 24. https://doi.org/10.1016/B978-081551500-5.50003-3

8. **Hou, B., Li, X., Ma, X., Du, C., Zhang, D., Zheng, M., Ma, F.** The Cost of Corrosion in China. Npj *Materials Degradation* 1 (1) 2017: pp. 4. https://doi.org/10.1038/s41529-017-0005-2

9. **Zhu, T., Wang, L., Sun, W., Yang, Z., Wang, S., Zhao, L., Liu, G.** Local Scaling of $CaCO_3$ on Carbon Steel Surface with Different Corrosion Types *Powder Technology* 356 2019: pp. 990 – 1000. https://doi.org/10.1016/j.powtec.2019.09.021

10. **Botello-Zubiate, M.E., Alvarez, A., Martínez-Villafañe, A., Almeraya-Calderon, F., Matutes-Aquino, J.A.** Influence of Magnetic Water Treatment on The Calcium Carbonate Phase Formation and The Electrochemical Corrosion Behavior of Carbon Steel *Journal of Alloys and Compounds* 369 (1 – 2) 2004: pp. 256 – 259. https://doi.org/10.1016/j.jallcom.2003.09.056

11. **Jain, A., Hautier, G., Ong, S.P., Moore, C.J., Fischer, C.C., Persson, K.A., Ceder, G.** Formation Enthalpies by Mixing GGA And GGA + U Calculations *Physical Review B – Condensed Matter and Materials Physics* 84 (4) 2011: pp. 045115. http://hdl.handle.net/1721.1/67053

12. **Ramkumar, T., Selvakumar, M., Mohanraj, M., Chandramohan, P., Narayanasamy, P.** Microstructure and Corrosion Behavior of ZnO-Mg Coating on AISI 4140 Steel Fabricated by Spray Coating *Journal of Materials Engineering and Performance* 29 2020: pp. 5796 – 5806. https://doi.org/10.1007/s11665-020-05099-9

13. **Zhang, Y.N., Zhang, S.G., Luo, J.H., Long, Y., Ji, N., Fan, B., Wang, S.M.** Effect of Flow Rate on the Corrosion Behavior of P110 Steel in High-Ca^{2+} and High-Cl^- Environment *Metals* 12 (7) 2022: pp. 1183. https://doi.org/10.3390/met12071183

14. **Xiong, Y., Zhang, A.** Corrosion Behavior of AZ80 Magnesium Alloy in Simulated Static and Dynamic Fluid Environments with Different pH Values *Journal of Materials Engineering and Performance* 32 (15) 2023: pp. 6915 – 6929. https://doi.org/10.1007/s11665-022-07591-w

15. **Singh, A.K., Zhou, L., Shinde, A., Suram, S.K., Montoya, J.H., Winston, D., Gregoire, J.M., Persson, K.A.** Electrochemical Stability of Metastable Materials *Chemistry of Materials* 29 (23) 2017: pp. 10159 – 10167. https://doi.org/10.1021/acs.chemmater.7b03980

16. **Patel, A.M., Nørskov, J.K., Persson, K.A., Montoya, J.H.** Efficient Pourbaix Diagrams of Many-Element Compounds *Physical Chemistry Chemical Physics* 21 (45) 2019: pp. 25323 – 25327. https://doi.org/10.1039/C9CP04799A

17. **Yu, B.L., Pan, X.L., Uan, J.Y.** Enhancement of Corrosion Resistance of Mg-9 Wt.% Al-1 Wt.% Zn Alloy by A Calcite ($CaCO_3$) Conversion Hard Coating *Corrosion Science* 52 (5) 2017: pp. 1874 – 1878. https://doi.org/10.1016/j.corsci.2010.01.014

18. **Wang, Y., Xiao, W., Dai, C., Wang, J., Pan, F.** Enhanced Corrosion Resistance of Mg Alloy Embedded in Cl--Containing Portland Cement with The Formation of CaCO3-Coated Mg (Al) O Passive Film Via One-Step Pulse Electrodeposition *Corrosion Science* 227 2024: pp. 111751. https://doi.org/10.1016/j.corsci.2023.111751